Ultrafast nonlinear optical spectroscopy of a dual-band negative index metamaterial all-optical switching device

Keshav M. Dani,[1,4] Zahyun Ku,[2,3,4] Prashanth C. Upadhya,[1] Rohit P. Prasankumar,[1] Antoinette J. Taylor,[1] and S. R. J. Brueck[2,*]

[1]*Center for Integrated Nanotechnologies, Los Alamos National Laboratory, Los Alamos, New Mexico 87545, USA*
[2]*Center for High Technology Materials and Electrical and Computer Engineering Department, University of New Mexico, Albuquerque, New Mexico 87106, USA*
[3]*Current Address: Air Force Research Laboratory, Wright-Patterson Air Force Base, Dayton, Ohio 45433, USA*
[4]*These authors contributed equally*
brueck@chtm.unm.edu

Abstract: We study the nonlinear optical response of a fishnet structure-metamaterial all-optical switching device that exhibits two near-infrared negative-index resonances. We study and compare the nonlinear optical response at both resonances and identify transient spectral features associated with the negative index resonance. We see a significantly stronger response at the longer wavelength resonance, but identical temporal dynamics at both resonances, providing insight into separately engineering the switching time and switching ratio of such a fishnet structure metamaterial all-optical switch. We also numerically reproduce the nonlinear behavior of our device using the Drude conductivity model and a finite integration technique over wide spectral and pump fluence ranges. Thereby, we show that beyond the linear properties of the device, the magnitude of the pump-probe response is completely described by only two material parameters. These results provide insight into engineering various aspects of the nonlinear response of fishnet structure metamaterials.

OCIS codes: (160.3918) Metamaterials; (240.6680) Surface plasmons; (310.6628) Subwavelength structures, nanostructures.

References and links

1. V. G. Veselago, "The electrodynamics of substances with simultaneously negative values of ε and μ," Sov. Phys. Usp. **10**(4), 509–514 (1968).
2. V. M. Shalaev, "Optical negative-index metamaterials," Nat. Photonics **1**(1), 41–48 (2007).
3. S. H. Lee, C. M. Park, Y. M. Seo, and C. K. Kim, "Reversed Doppler effect in double negative metamaterials," Phys. Rev. B **81**(24), 241102 (2010).
4. D. Schurig, J. J. Mock, B. J. Justice, S. A. Cummer, J. B. Pendry, A. F. Starr, and D. R. Smith, "Metamaterial electromagnetic cloak at microwave frequencies," Science **314**(5801), 977–980 (2006).
5. J. Valentine, J. Li, T. Zentgraf, G. Bartal, and X. Zhang, "An optical cloak made of dielectrics," Nat. Mater. **8**(7), 568–571 (2009).
6. J. B. Pendry, "Negative refraction makes a perfect lens," Phys. Rev. Lett. **85**(18), 3966–3969 (2000).
7. H.-T. Chen, W. J. Padilla, J. M. O. Zide, A. C. Gossard, A. J. Taylor, and R. D. Averitt, "Active terahertz metamaterial devices," Nature **444**(7119), 597–600 (2006).
8. H. Tao, A. C. Strikwerda, K. Fan, W. J. Padilla, X. Zhang, and R. D. Averitt, "Reconfigurable terahertz metamaterials," Phys. Rev. Lett. **103**(14), 147401 (2009).
9. M. Lapine, D. Powell, M. Gorkunov, I. Shadrivov, R. Marqués, and Y. Kivshar, "Structural tunability in metamaterials," Appl. Phys. Lett. **95**(8), 084105 (2009).
10. E. Kim, Y. R. Shen, W. Wu, E. Ponizovskaya, Z. Yu, A. M. Bratkovsky, S. Wang, and R. S. Williams, "Modulation of negative index metamaterials in the near-IR range," Appl. Phys. Lett. **91**(17), 173105 (2007).
11. T. Driscoll, H. T. Kim, B. G. Chae, B. J. Kim, Y. W. Lee, N. M. Jokerst, S. Palit, D. R. Smith, M. Di Ventra, and D. N. Basov, "Memory metamaterials," Science **325**(5947), 1518–1521 (2009).
12. K. M. Dani, Z. Ku, P. C. Upadhya, R. P. Prasankumar, S. R. Brueck, and A. J. Taylor, "Subpicosecond optical switching with a negative index metamaterial," Nano Lett. **9**(10), 3565–3569 (2009).

#137930 - $15.00 USD Received 9 Nov 2010; revised 7 Feb 2011; accepted 10 Feb 2011; published 15 Feb 2011

Report Documentation Page

Form Approved
OMB No. 0704-0188

1. REPORT DATE	2. REPORT TYPE	3. DATES COVERED
15 FEB 2011		**00-00-2011 to 00-00-2011**

4. TITLE AND SUBTITLE	5a. CONTRACT NUMBER
Ultrafast nonlinear optical spectroscopy of a dual-band negative index metamaterial all-optical switching device	5b. GRANT NUMBER
	5c. PROGRAM ELEMENT NUMBER
6. AUTHOR(S)	5d. PROJECT NUMBER
	5e. TASK NUMBER
	5f. WORK UNIT NUMBER
7. PERFORMING ORGANIZATION NAME(S) AND ADDRESS(ES) **University of New Mexcio,Department of Electrical and Computer Engineering ,Center for High Technology Materials,Albuquerque,NM,87106**	8. PERFORMING ORGANIZATION REPORT NUMBER
9. SPONSORING/MONITORING AGENCY NAME(S) AND ADDRESS(ES)	10. SPONSOR/MONITOR'S ACRONYM(S)
	11. SPONSOR/MONITOR'S REPORT NUMBER(S)

12. DISTRIBUTION/AVAILABILITY STATEMENT
Approved for public release; distribution unlimited

13. SUPPLEMENTARY NOTES

14. ABSTRACT

We study the nonlinear optical response of a fishnet structuremetamaterial all-optical switching device that exhibits two near-infrared negative-index resonances. We study and compare the nonlinear optical response at both resonances and identify transient spectral features associated with the negative index resonance. We see a significantly stronger response at the longer wavelength resonance, but identical temporal dynamics at both resonances, providing insight into separately engineering the switching time and switching ratio of such a fishnet structure metamaterial all-optical switch. We also numerically reproduce the nonlinear behavior of our device using the Drude conductivity model and a finite integration technique over wide spectral and pump fluence ranges. Thereby, we show that beyond the linear properties of the device, the magnitude of the pump-probe response is completely described by only two material parameters. These results provide insight into engineering various aspects of the nonlinear response of fishnet structure metamaterials.

15. SUBJECT TERMS

16. SECURITY CLASSIFICATION OF:			17. LIMITATION OF ABSTRACT	18. NUMBER OF PAGES	19a. NAME OF RESPONSIBLE PERSON
a. REPORT **unclassified**	b. ABSTRACT **unclassified**	c. THIS PAGE **unclassified**	**Same as Report (SAR)**	**11**	

13. D. J. Cho, W. Wu, E. Ponizovskaya, P. Chaturvedi, A. M. Bratkovsky, S. Y. Wang, X. Zhang, F. Wang, and Y. R. Shen, "Ultrafast modulation of optical metamaterials," Opt. Express **17**(20), 17652–17657 (2009).
14. S. Zhang, W. Fan, N. C. Panoiu, K. J. Malloy, R. M. Osgood, and S. R. J. Brueck, "Experimental demonstration of near-infrared negative-index metamaterials," Phys. Rev. Lett. **95**(13), 137404 (2005).
15. Z. Ku, and S. R. J. Brueck, "Comparison of negative refractive index materials with circular, elliptical and rectangular holes," Opt. Express **15**(8), 4515–4522 (2007).
16. D. Xia, Z. Ku, S. C. Lee, and S. R. J. Brueck, "Nanostructures and functional materials fabricated by interferometric lithography," Adv. Mater. (Deerfield Beach Fla.) **23**(2), 147–179 (2011).
17. S. Zhang, W. Fan, K. J. Malloy, S. R. J. Brueck, N.-C. Panoiu, and R. M. Osgood, "Near-infrared double negative metamaterials," Opt. Express **13**(13), 4922–4930 (2005).
18. C. S. T. Studio Suite 18, *http://www.cst.com*.
19. P. B. Johnson, and R. W. Christy, "Optical constants of the noble metals," Phys. Rev. B **6**(12), 4370–4379 (1972).
20. Z. Ku, and S. R. J. Brueck, "Experimental demonstration of sidewall angle induced bianisotropy in multiple layer negative index metamaterials," Appl. Phys. Lett. **94**(15), 153107 (2009).
21. Z. Ku, J. Zhang, and S. R. J. Brueck, "Bi-anisotropy of multiple-layer fishnet negative-index metamaterials due to angled sidewalls," Opt. Express **17**(8), 6782–6789 (2009).
22. Z. Ku, K. M. Dani, P. C. Upadhya, and S. R. J. Brueck, "Bianisotropic negative-index metamaterial embedded in a symmetric medium," J. Opt. Soc. Am. B **26**(12), B34–B38 (2009).
23. A. Mary, S. G. Rodrigo, F. J. Garcia-Vidal, and L. Martin-Moreno, "Theory of negative-refractive-index response of double-fishnet structures," Phys. Rev. Lett. **101**(10), 103902 (2008).
24. P. M. Fauchet, D. Hulin, R. Vanderhaghen, A. Mourchid, and W. L. Nighan, Jr., "The properties of free carriers in amorphous silicon," J. Non-Cryst. Solids **141**, 76–87 (1992).
25. A. Mourchid, R. Vanderhaghen, D. Hulin, C. Tanguy, and P. M. Fauchet, "Femtosecond optical spectroscopy in a-Si:H and its alloys," J. Non-Cryst. Solids **114**, 582–584 (1989).
26. A. Esser, K. Seibert, H. Kurz, G. N. Parsons, C. Wang, B. N. Davidson, G. Lucovsky, and R. J. Nemanich, "Ultrafast recombination and trapping in amorphous silicon," Phys. Rev. B Condens. Matter **41**(5), 2879–2884 (1990).
27. I. A. Shkrob, and R. A. Crowell, "Ultrafast charge recombination in undoped amorphous hydrogenated silicon," Phys. Rev. B **57**(19), 12207–12218 (1998).
28. M. Dressel, and G. Gruner, *Electrodynamics of Solids* (Cambridge University Press, 2002), Chap. 5.
29. J. Singleton, *Band Theory and Electronic Properties of Solids* (Oxford University Press, 2001), Chap. 9.3.
30. P. M. Fauchet, D. Hulin, R. Vanderhaghen, A. Mourchid, and W. L. Nighan, Jr., "The properties of free carriers in amorphous silicon," J. Non-Cryst. Solids **141**, 76–87 (1992).
31. J. I. Pankove, *Hydrogenated Amorphous Silicon* (Academic Press, 1984).
32. R. A. Street, *Hydrogenated Amorphous Silicon* (Cambridge University Press, 1991).
33. T. Y. Choi, D. J. Hwang, and C. P. Grigoropoulos, "Ultrafast laser-induced crystallization of amorphous silicon films," Opt. Eng. **42**(11), 3383–3388 (2003).
34. K. Sokolowski-Tinten, and D. Von der Linde, "Generation of dense electron-hole plasmas in silicon," Phys. Rev. B **61**(4), 2643–2650 (2000).

1. Introduction

Metamaterials are artificially fabricated composites consisting of sub-wavelength sized structures that demonstrate novel linear optical properties like negative index of refraction, reverse Doppler effect and energy propagation opposite to the wave vector of the electromagnetic wave [1–3]. They also promise intriguing applications such as optical cloaking [4,5] and perfect lensing [6]. Recently, the active modulation of such optical properties by applying bias fields [7], heat [8], mechanical motion [9] or electromagnetic pulses [10] has created much interest in the development of photonic applications and devices. For example, devices where thermally activated mechanical motion tunes the resonant optical properties have been demonstrated for applications in thermal sensing [8]. Similarly, electrically controlled persistent frequency tuning of metamaterials has created a new class of memory metamaterials for applications in memory devices [11]. In particular, the active modulation of the optical properties with an electromagnetic pulse has special significance for photonic applications as well as for the development of nonlinear optical materials.

Recent experiments have shown that one can modulate the optical properties of a metamaterial on a sub-picosecond timescale enabling ultrafast photonic devices [12,13]. Along these lines, metamaterial devices with the potential of terabits per second all-optical communication – two orders of magnitude faster than previously achieved have been demonstrated. In these demonstrations, the authors used a fishnet structure metamaterial [14,15] with two negative index resonances in the near-infrared (IR) corresponding to two different periodic wavevectors of the internal gap-mode surface plasmon polaritons (IG-SPP)

#137930 - $15.00 USD Received 9 Nov 2010; revised 7 Feb 2011; accepted 10 Feb 2011; published 15 Feb 2011

[12]. A deeper understanding of the nonlinear optical properties of such dual-band fishnet structure devices is important for the further development and optimization of nonlinear metamaterials in the near-IR as well as for ultrafast optical metamaterial devices. Such an understanding can lead to devices with more efficiency, a broader frequency range of operation and added functionality.

In this letter, we describe the results obtained by performing optical pump-probe spectroscopy on such a fishnet structure metamaterial device that has two negative index resonances in the near-IR, associated with different Fourier components of the metamaterial structure. We photoexcite the metamaterial with a visible pump pulse and then measure the pump-induced, time-resolved change in transmission ($\Delta T/T$) with a time-delayed near-IR probe pulse around both the resonances as a function of probe wavelength, pump fluence and probe polarization. We identify a clear transient spectral feature associated with the resonant negative-index responses. We observe that the longer wavelength resonance has a significantly stronger nonlinear response ($\Delta T/T$~70%) corresponding to its larger absolute value of the negative index and the stronger Drude response of photocarriers at longer wavelengths. However, in contrast to the change in magnitude, the temporal dynamics of the nonlinear response are identical at both resonances. As a function of pump fluence, the switching ratio (SR) scales nonlinearly, but identically, for both the resonances. This identical scaling demonstrates the common physical origin of the metamaterial optical nonlinearity at both resonances, while the nonlinear scaling of the SR versus pump fluence provides insight into the dependence of fishnet structure properties on its constituent elements. We numerically calculate the nonlinear response of our device using the Drude conductivity model for the properties of the photoexcited dielectric layer and then employ a finite integration technique (FIT) for the effective parameters of the metamaterial from its constituent elements. Our simulations reproduce the nonlinear response over a wide spectral range and a decade in pump fluence. The model demonstrates that beyond the linear properties of the device, the magnitude of the nonlinear response over this wide range of experimental parameters is determined by only two material parameters – the effective mass and the scattering rate of the photoexcited carriers in the α-Si layer. These results elucidate the fundamental nonlinear optical properties of fishnet structure metamaterials in the near-IR; and their utility in ultrafast optical devices.

2. Design and fabrication

The dual-band metamaterial device reported here is composed of a BK7 glass substrate and a single metal-dielectric-metal (Ag/α-Si/Ag) functional layer with an inter-penetrating two-dimensional square array of elliptical apertures. The geometrical parameters of the device are indicated in Fig. 1. The orthogonal pitches of the two-dimensional grating are both fixed at 345 nm (p). The thickness of the silver (Ag) and amorphous silicon (α-Si) films are fixed at 28 nm and 68 nm, respectively. The elliptical aperture size ($2a_x$, $2a_y$) is formed with lengths of $0.69 \cdot p$ (238 nm) and $0.47 \cdot p$ (162 nm) in the major and minor axis, respectively as shown in Fig. 1. The fabrication process for the device has been described in detail elsewhere [12,16].

#137930 - $15.00 USD Received 9 Nov 2010; revised 7 Feb 2011; accepted 10 Feb 2011; published 15 Feb 2011

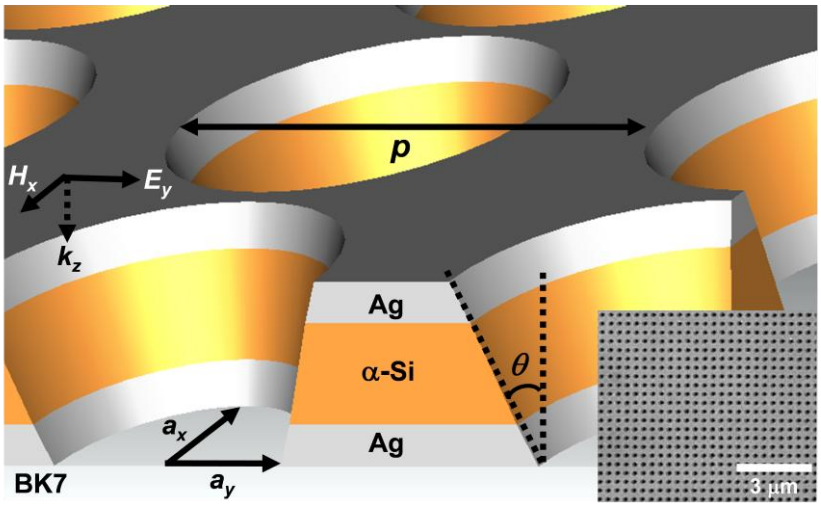

Fig. 1. Schematic view of fishnet structure-metamterial device. Geometrical parameters of elliptical negative-index metamaterial: p = 345 nm; a_x = 119 nm; a_y = 81 nm; and θ (sidewall-angle) = 18°. The device consists of 28 nm thick Ag; 68 nm thick α-Si; and 28 nm thick Ag. The direction of polarization for the incoming light is parallel to the narrower stripe width between apertures. Inset: Top view scanning electron microscope (SEM) image.

3. Linear optical properties

The normal incidence transmission through the metamaterial device was recorded with a Nicolet Fourier transform infrared (FTIR) spectrometer with a quartz beam splitter and a DTGS-KBr detector and normalized to the transmission of a bare BK7 glass substrate. Given the elliptical geometry of the holes in our device [12,15], the device response is different for the two polarizations. For the geometry shown in Fig. 1, (E field parallel to the minor axis), we denote the polarization by $E_{\|}$. The E-field perpendicular to the minor axis of the holes is then denoted by $E_{\perp}$. The metamaterial device is designed to have strong negative index resonances for $E_{\|}$. The measured transmission curves for $E_{\|}$ (black squares) and for $E_{\perp}$ (red squares) are shown in Fig. 2(a). For $E_{\|}$ we see large overall transmission with characteristic dips associated with the negative index resonances [14,15]. For $E_{\perp}$, the electric field sees a metamaterial geometry with a larger width of the continuous wires (more negative permittivity) and the magnetic field sees a shorter width of the split wire pair (less negative permeability) [17]. This results in refractive negative index resonances that are of lower quality and shifted in frequency. Thus, the overall transmission for $E_{\perp}$ is significantly lower with barely discernible dips that are shifted in frequency from the $E_{\|}$ resonances.

To understand our experimental results, we performed simulations of our device using CST Microwave Studio [18] based on a finite integration technique. We assumed perfect electric conductor (PEC) and perfect magnetic conductor (PMC) boundary conditions between unit cells to stimulate transverse electromagnetic (TEM) plane wave propagation in the z direction. The optical parameters for the constitutive materials were taken as $n_{\text{substrate}}$ = 1.5 and n_{MgF2} = 1.38, where MgF_2 is used as the protection layer [12]. The refractive index of α-Si was taken as $n_{\alpha\text{-Si}}$ = 3.35. A Drude model for the Ag dielectric function was used with ω_p (plasma frequency) = 9.02 eV and ω_c (scattering frequency) = 0.042 eV [19]. This scattering frequency is increased by a factor of two compared to that of bulk silver to account for additional scattering mechanisms in this polycrystalline thin film, in addition to sample inhomogeneity across the ~mm^2 measurement area associated with the FTIR beam [15]. These parameters produce the best fit between experiment and simulation of the transmission through our device for $E_{\|}$ over the wavelength range of interest (1 to 2 μm), as shown in Fig.

#137930 - $15.00 USD Received 9 Nov 2010; revised 7 Feb 2011; accepted 10 Feb 2011; published 15 Feb 2011

2(a). The measured transmission for $E_{\perp}$ is also closely reproduced by the simulation with these same parameters.

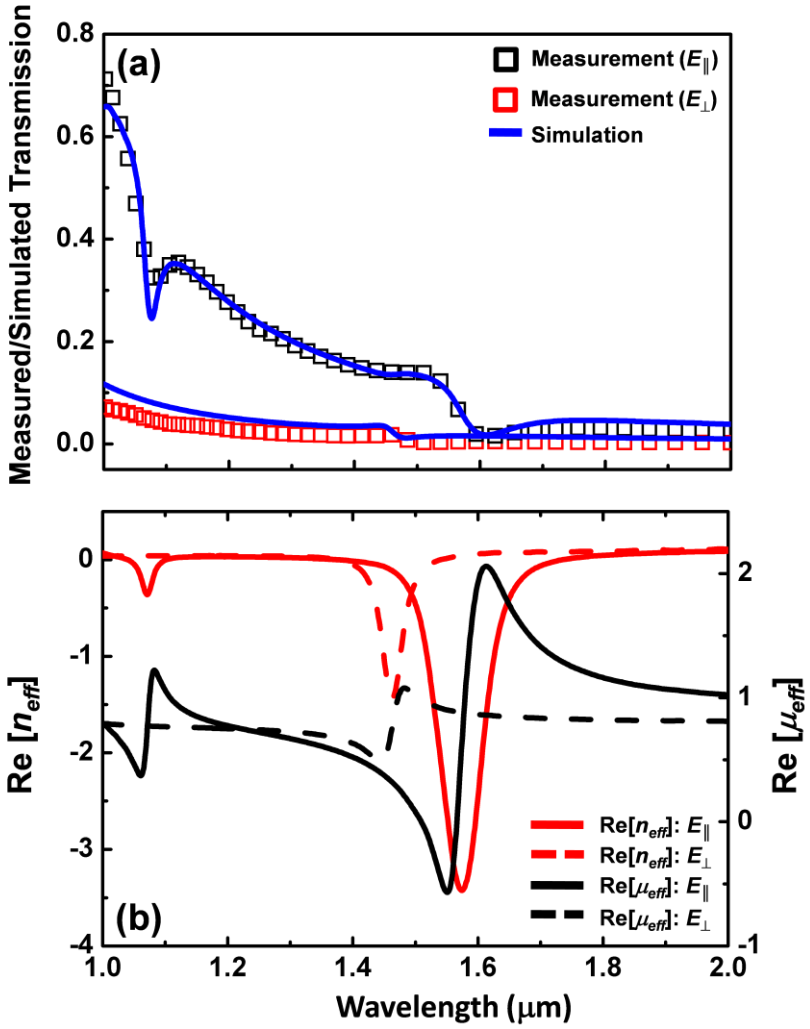

Fig. 2. (a) Measured normal incidence transmission spectra (FTIR) for both polarizations ($E_{\parallel}$ and $E_{\perp}$). The simulated transmission curves are obtained using a finite integration technique, where the metamaterial parameters are adjusted to give the best fit to the measured transmission. (b) Real parts of the effective refractive index and permeability using the best-fit parameters obtained from (a).

Based on the above metamaterial structure, we extract the effective parameters, including the index of refraction and permeability as shown in Fig. 2(b). We note that, as a result of the structural asymmetry, i.e. the nonzero sidewall-angle (θ = 18°) due to fabrication imperfections as shown in Fig. 1, modified retrieval method is needed to extract the effective parameters rather than the standard method associated with a symmetric structure along the propagation direction. For further details of this methodology, see Refs. [20–22].

Figure 2(b) shows the real parts of the extracted effective refractive index (n_{eff}) and permeability (μ_{eff}) from 1 to 2 μm for $E_{\parallel}$ (solid curves). We see two negative index resonances at ~1.06 μm and ~1.58 μm corresponding to the (1,0) and (1,1) k-vectors of the periodicity of the 2D hole structure. The resonances are related to the coupling to the IG-SPPs, which gives rise to a magnetic response and permeability [23]. The magnetic field profiles through the

#137930 - $15.00 USD Received 9 Nov 2010; revised 7 Feb 2011; accepted 10 Feb 2011; published 15 Feb 2011

middle of the device at the corresponding resonant wavelengths show the first and second IG-SPP modes (not shown here) [12]. Therefore, the longer wavelength coupling mode is associated with IG-SPP (1,0) due to the configuration between nearest apertures, e.g. periodicity (p). On the other hand, the shorter wavelength coupling mode is related to IG-SPP (1,1) owing to the coupling along the diagonals ($p/\sqrt{2}$). Figure 2(b) also shows the real parts of the extracted effective refractive index (n_{eff}) for $E_{\perp}$. As expected, we see a diminished and frequency-shifted fundamental resonance for $E_{\perp}$, corresponding to the barely discernible dip in transmission [14]. As a result of the weak negative index resonance, we also observe a weak nonlinear response when the probe polarization is $E_{\perp}$. We now turn our attention to a detailed study of the pump-probe response of the device with the probe polarization set to $E_{\parallel}$.

4. Pump probe setup

The nonlinear response of our device is measured with a multi-color pump-probe experiment. We use a visible pump pulse (590 nm) to photoexcite carriers above the bandgap of the α-Si dielectric material (~700 nm) and a near-IR probe pulse to measure the pump-induced change in transmission at the two resonances. To generate the visible pump and near-IR probe, we start with a commercial 100 kHz regenerative amplifier with sub-60 fs, 10 μJ/cm^2 and 800 nm pulses to simultaneously seed two optical parametric amplifiers (OPAs), one operating in the visible and one in the near-IR as shown in Fig. 3. The signal pulse from the near-IR OPA is tuned to 1180 nm and then frequency doubled to produce the 590 nm visible pump pulse. The idler pulse from the visible OPA can range from 930 to 2300 nm and is tuned to probe the device response over the entire near-IR range. This unconventional experimental arrangement, where the visible OPA produces the near-IR probe and the near-IR OPA produces the visible pump, allows us to access the response of the device over both negative index resonances, while avoiding the degeneracy point at 1.6 μm of the near-IR OPA.

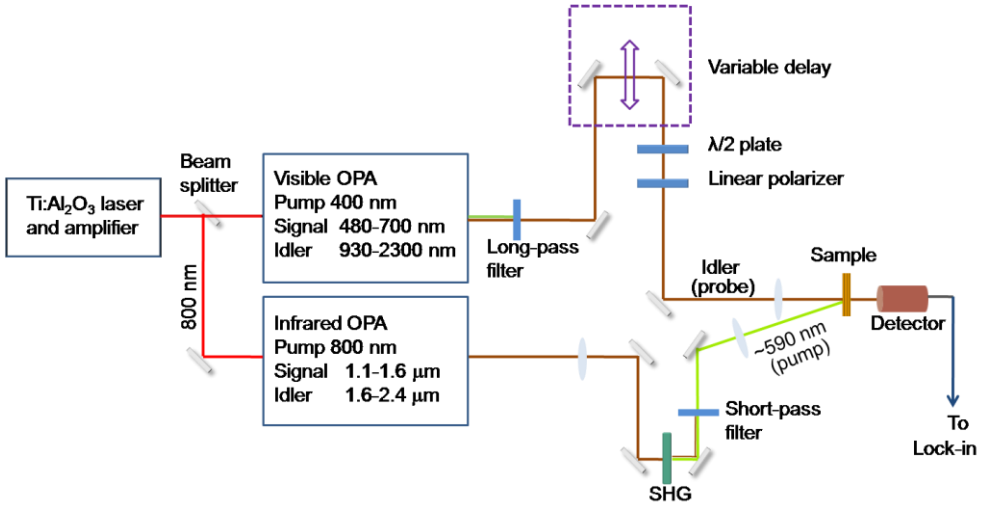

Fig. 3. Ultrafast pump-probe setup. The frequency doubled signal pulse from a near-IR OPA provides the 590 nm visible pump pulse. The idler pulse from a visible OPA (930-2300 nm) is tuned to study the response around each resonance.

The SR, i.e. the pump-induced relative change in transmission ($\Delta T/T$) is measured by mechanically chopping the pump beam at 4 kHz and measuring the resulting modulation of the transmission of the probe beam using a lock-in amplifier. In order to ensure that we study only pump-induced effects, the probe power (typically 30 μW) is kept significantly lower than the pump power (7.0-0.5 mW). Further, the probe spot size (~30 μm) is kept much smaller than the pump spot size (~100 μm) so as to sample only the central uniformly photoexcited

#137930 - $15.00 USD Received 9 Nov 2010; revised 7 Feb 2011; accepted 10 Feb 2011; published 15 Feb 2011

density generated by the pump. In this configuration, we study the nonlinear response of our device as a function of probe wavelength, pump fluence and probe polarization.

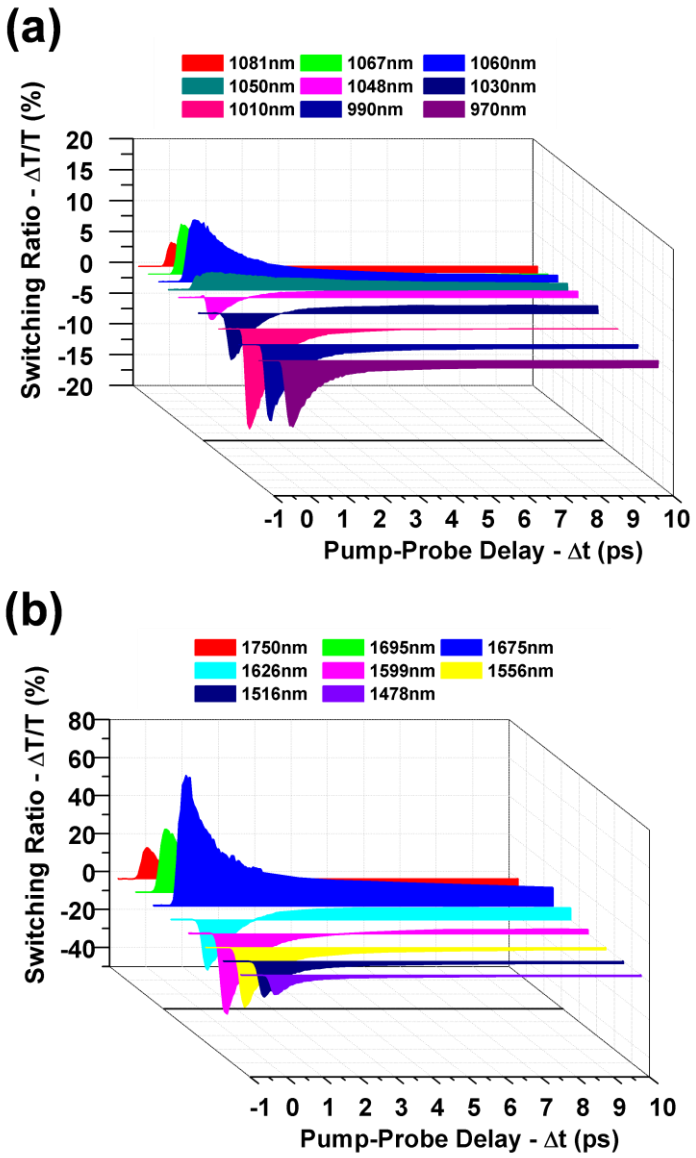

Fig. 4. Time-resolved pump-probe response versus probe wavelength. (a) Response near the (1,1) resonance (b) Response near the (1,0) resonance. At both resonances and for all probe wavelengths, the time-resolved traces show a triple exponential decay with a fast ~600 fs component, a few ps component and a slow component that lasts for nanoseconds. At both resonances, at zero pump-probe delay we see $\Delta T/T > 0$ ($\Delta T/T < 0$) for probe wavelengths just longer (shorter) that the negative index resonance.

5. Probe wavelength dependence

Figure 4 displays the time-resolved SR ($\Delta T/T$) versus pump-probe delay for different probe wavelengths around (a) the (1,1) and (b) the (1,0) resonance respectively. At all wavelengths around both resonances (and as reported previously for the (1,1) resonance [12]), we see a triple exponential decay consisting of a fast 600 femtosecond component, an intermediate few

#137930 - $15.00 USD Received 9 Nov 2010; revised 7 Feb 2011; accepted 10 Feb 2011; published 15 Feb 2011

picosecond component and a background signal lasting longer than a few nanoseconds. Over 80% of the SR is due to the fast 600 femtosecond component, thereby enabling a sub-picosecond all-optical switch operation at either resonance. At both resonances, we observe $\Delta T/T > 0$ ($\Delta T/T < 0$) for wavelengths longer (shorter) than the resonance. By plotting the peak SR at zero pump-probe delay versus the probe wavelength as shown in Fig. 5, we observe a clear 'S-shaped' feature at each of the two negative index resonances. We note that unstructured layers of Ag or α-Si do not display such an 'S-shaped' dependence of the peak pump probe signal versus probe wavelength. Moreover, $\Delta T/T$ for such unstructured layers of Ag or α-Si is ~1%, as opposed to the much larger SRs with the metamaterial sample. The enhancement of the nonlinear response by a factor of about 70 in metamaterials is a direct result the coupling to the metamaterial structural resonance.

This response of the metamaterial can be understood as due to the photoexcitation of carriers into the α-Si layer of the metamaterial by the pump pulse. The presence of photoexcited carriers in the α-Si layer impacts the resonant *LC* permeability of the fishnet structure and modifies its optical response towards that of a single metal sheet on a substrate. As the photocarriers decay, the device recovers to its original negative index behavior. Pump-probe measurements under identical experimental conditions on an unstructured layer of α-Si show decay dynamics similar to the metamaterial device – a fast 600 fs component, an intermediate few ps component and a much longer component of 100s of ps, thus confirming that the dynamics in α-Si determines the dynamics of the metamaterial [12]. Previous extensive studies of the carrier dynamics of α-Si have attributed the multiple decay components to processes like Auger recombination, carrier trapping and cooling [24–27]. We note that the identical temporal dynamics at both resonances, despite their different frequency, different geometry of the underlying negative index resonances and different magnitude of the nonlinear response, suggests that the switching time of such a metamaterial based all-optical device can be engineered independent of other device properties, e.g. SR and frequency of operation.

To quantitatively understand the change in refractive index of the α-Si due to photoexcitation, we apply the Drude conductivity model [28]:

$$n_{photoexcited\ \alpha-Si} = \left[n_{\alpha-Si}^2 - \frac{{\omega_p}^2}{\omega(\omega + i\gamma)} \right]^{1/2} \tag{1}$$

where $\omega_p = \left(e^2 N / \varepsilon_0 m^*\right)^{1/2}$ is the plasma frequency, ω – angular frequency of probe light, m^* – effective mass, ε_0 – permittivity of free space, N – photoexcited carrier density and γ – the scattering rate. We use $m^* = 0.3m_0$ (where m_0 is the mass of a free electron) and γ^{-1}~1.5 fs to obtain $n_{\text{photoexcited α-Si}}$ over the 1-2 μm wavelength range, which is then used to calculate the effective parameters of the metamaterial device with CST Microwave Studio, as was done for the unphotoexcited α-Si case [29–34]. The photoexcitation density ($N = 1.23 \times 10^{20}$ cm^{-3}) is obtained from the pump fluence of 0.9 mJ/cm^2 while taking into consideration the 30% absorption of the pump pulse (60% reflection and 10% transmission).

#137930 - $15.00 USD Received 9 Nov 2010; revised 7 Feb 2011; accepted 10 Feb 2011; published 15 Feb 2011

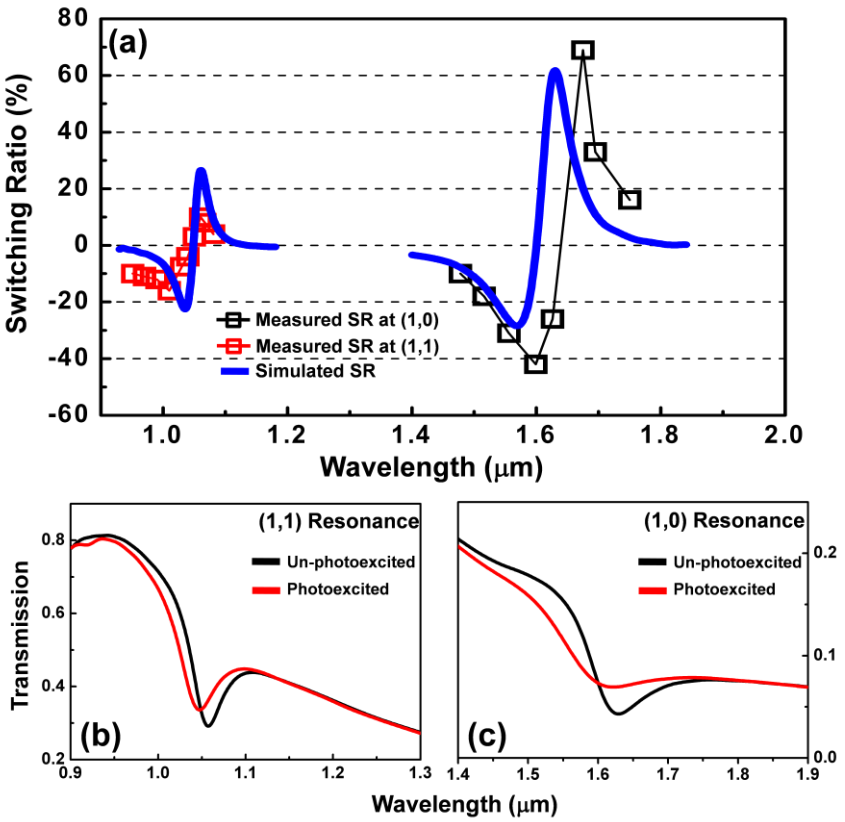

Fig. 5. Dual-band negative index resonance in a single metamaterial device. (a) We see the characteristic pump-probe response of a negative index resonance in a metamaterial device, thereby allowing us to clearly identify two negative index resonances in our device. The simulated transmission through the device on photoexcitation around the (b) (1,1) resonance and (c) (1,0) resonance demonstrate that $\Delta T/T > 0$ ($\Delta T/T < 0$) for wavelengths just longer (shorter) than the negative index resonance.

Figures 5(b) and (c) show the transmission through the metamaterial device over the 1- to 2-μm range for the cases of a photoexcited (red) and an un-photoexcited (black) α-Si layer. For wavelengths just above (below) the negative index resonance, we observe increased (decreased) transmission following photoexcitation. Thus, the pump-probe signal at zero time delay versus probe wavelength exhibits an 'S-shaped' feature at the negative index resonance. Figure 5(a) compares this measured and simulated pump-probe response at zero time delay over the 1-2 μm wavelength range, indicating good agreement between experiment and theory.

In Fig. 5a, we observe significantly higher SRs at the longer wavelength (1,0)-resonance (+ 70% and −40% for the positive and negative peaks respectively) versus the shorter wavelength (1,1)-resonance (+ 10% and −18%). This stronger nonlinear response is a result of the larger absolute value of the negative index at the (1,0)-resonance and the stronger Drude response of photocarriers at longer wavelengths. From a technological standpoint, larger SRs are important for reduced errors in all-optical communication as well as reduced energy requirements. We note here that our analytical model demonstrates that given a fixed device geometry (and hence its linear properties), the nonlinear response is completely described by only two material parameters – m_0 and γ. This provides simple and straightforward insights into engineering the magnitude of the nonlinear response of fishnet structure metamaterials.

#137930 - $15.00 USD Received 9 Nov 2010; revised 7 Feb 2011; accepted 10 Feb 2011; published 15 Feb 2011

6. Pump fluence dependence

We measure the SR versus pump fluence for two fixed probe wavelengths (1640 nm and 1010 nm) corresponding to points near the peak positive response for the (1,0) resonance and the peak negative response for the (1,1) resonance (Fig. 5a). Figure 6 shows the peak SR versus pump fluence for the two resonances. At both wavelengths, the SR scales nonlinearly, but identically (see the inset of Fig. 6) with the fluence, thus demonstrating experimentally the common physical origin of the pump-probe response, i.e. the change in effective parameters of the metamaterial at either resonance is due to the presence of photocarriers in the α-Si dielectric layer.

Again, we quantitatively understand the nonlinear scaling of the SR with the pump fluence by using the Drude model [Eq. (1)] with the same parameters ($m^* = 0.3m_0$, $\gamma^{-1} \sim 1.5$ fs) to obtain the refractive index of the photoexcited α-Si at each of the two wavelengths (1640 nm and 1010 nm). This value of $n_{\text{photoexcited α-Si}}$ then gives us the effective parameters of the metamaterial device. Figure 6 shows the agreement of the numerical simulation (blue curves) to the experimental data around the two resonant wavelengths. We point out that the pump fluences in our experiment are small enough that the change in the refractive index of the α-Si on photoexcitation as given by Eq. (1) is linear in the photoexcitation density. The nonlinear scaling of the SR is therefore a result of a nonlinear dependence of n_{eff} on $n_{\text{photoexcited α-Si}}$. This scaling enables us to estimate pump energy requirements for higher SRs for applications in ultrafast all-optical switching. A further understanding of this phenomenon is also important for metamaterial applications such as sensing and for the field of active metamaterials in general, where small changes in the constituent elements are required to produce large, nonlinear changes in the effective parameters of the metamaterial.

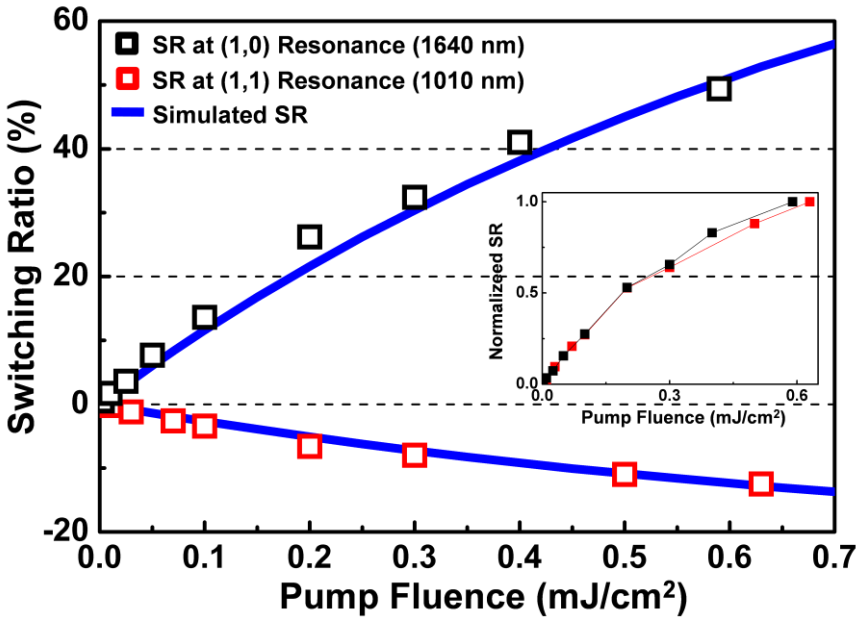

Fig. 6. SR versus pump fluence. We see a nonlinear scaling of the SR versus pump fluence at both the resonances. This is indicative of the nonlinear dependence of the effective parameters of the metamaterial on its constituent elements. Inset: The normalized plots show that the scaling is identical for both the resonances, thereby demonstrating experimentally the common physical origin of the nonlinear response at both the resonances, i.e. the change in metamaterial properties is due to the photoexcitation of carriers in the α-Si.

#137930 - $15.00 USD Received 9 Nov 2010; revised 7 Feb 2011; accepted 10 Feb 2011; published 15 Feb 2011

7. Conclusion

Using pump-probe spectroscopy, we studied the ultrafast nonlinear optical response of a metamaterial device exhibiting two negative index resonances in the near-IR. The study and comparison of the nonlinear response of both resonances in a single device provides insight into engineering various aspects of the nonlinear optical properties of the metamaterial including: magnitude of the pump probe response, resonant frequency and temporal dynamics. These in turn have technological implications in engineering the switching ratio, frequency of operation and switching time of an all-optical metamaterial switching device. By photoexcitation of carriers in the α-Si dielectric layer of the metamaterial, we altered the transmission at both resonances on a sub-picosecond timescale. We identified an 'S-shaped' spectral feature in the pump-probe response of the resonances associated with a negative index. We studied the nonlinear optical response of the device at both resonances as a function of probe wavelength, pump fluence and probe polarization. We observed much higher switching ratios at the (1,0) resonance (~ + 70%) relative to the (1,1) resonance (~ + 10%) corresponding to the larger absolute value of the negative index and the stronger Drude response of photocarriers at longer wavelengths. In contrast, both resonances show identical temporal dynamics independent of the different geometries and frequencies of the negative index resonances. This suggests that in principle one can engineer the switching time of an all-optical device independently of its linear properties, frequency of operation and switching ratio. We also saw a nonlinear, but identical, scaling of the switching ratio versus pump fluence for both resonances. This nonlinear scaling demonstrates the nonlinear dependence of the effective parameters of the metamaterial on its constituent elements. We understood and numerically reproduced the experimental data using a Drude conductivity model for the photocarriers in α-Si and a finite integration technique for the effective parameters of the metamaterial device. We obtained very good agreement with the experiment over a wide spectral range and over decade variation in pump fluence. Our model indicates that the magnitude of the pump-probe signal can be completely understood via only two material parameters – the effective mass and the scattering rate of the photoexcited carriers in α-Si. This study provides deeper insight into the ultrafast nonlinear properties of fishnet metamaterials and their utility for near-IR photonic devices like ultrafast optical switches.

Acknowledgments

The UNM portion of this work was supported by the Defense Advanced Research Projects Agency (DARPA) under the University Photonics Research Center program. The LANL portion of this work was performed at the Center for Integrated Nanotechnologies, a U.S. Department of Energy, Office of Basic Energy Sciences user facility and also partially supported by the LANL's Laboratory Directed Research and Development Program. Los Alamos National Laboratory, an affirmative action equal opportunity employer, is operated by Los Alamos National Security, LLC, for the National Nuclear Security Administration of the U.S. Department of Energy under Contract No. DE-AC52-06NA25396.

#137930 - $15.00 USD Received 9 Nov 2010; revised 7 Feb 2011; accepted 10 Feb 2011; published 15 Feb 2011